CHEMISTRY
A European Journal

Supporting Information

Polyol Solvation Effect on Tuning the Universal Growth of Binary Metal Oxide Nanodots@Graphene Oxide Heterostructures for Electrochemical Applications

Shuangshuang Tan, Yexin Pan, Qiulong Wei, Yalong Jiang, Fangyu Xiong, Xuhui Yao, Zhijun Cai, Qinyou An, Liang Zhou, and Liqiang Mai*[a]

chem_201902697_sm_miscellaneous_information.pdf

Table S1. The physic-chemical parameters of a series of alcohols solvents, including permittivity (20℃), surface tension (20℃, N/m), dipole moment (C·m) and viscosity (20℃, mPa · s).

| Solvents	Permittivity (20℃)	Surface tension (20℃, N/m)	Viscosity (20℃, mPa·s)	Dipole moment (C·m)	Boiling point (℃)
H₂O	80.1	$72.58*10^{-3}$	1	$6.47*10^{-30}$	100
methanol	31.2	$22.55*10^{-3}$	0.5945	$5.55*10^{-30}$	64.7
alcohol	25.7	$22.27*10^{-3}$	1.17	$5.60*10^{-30}$	78
n-propanol	22.2	$23.8*10^{-3}$	2.26	$5.53*10^{-30}$	97.1
butanol	17.1	$24.6*10^{-3}$	2.95	$5.60*10^{-30}$	117.25
octanol	10.34	$26.06*10^{-3}$	8.93	$5.60*10^{-30}$	196
glycol	38.66	$46.49*10^{-3}$	21.38	$7.34*10^{-30}$	197.3
1,2-propanediol	32	$72*10^{-3}$	56	$7.51*10^{-30}$	188.2
1,3-butanediol	?	$37.8*10^{-3}$	130.3	?	207
glycerol	42.5	$63.3*10^{-3}$	1412	?	290.9
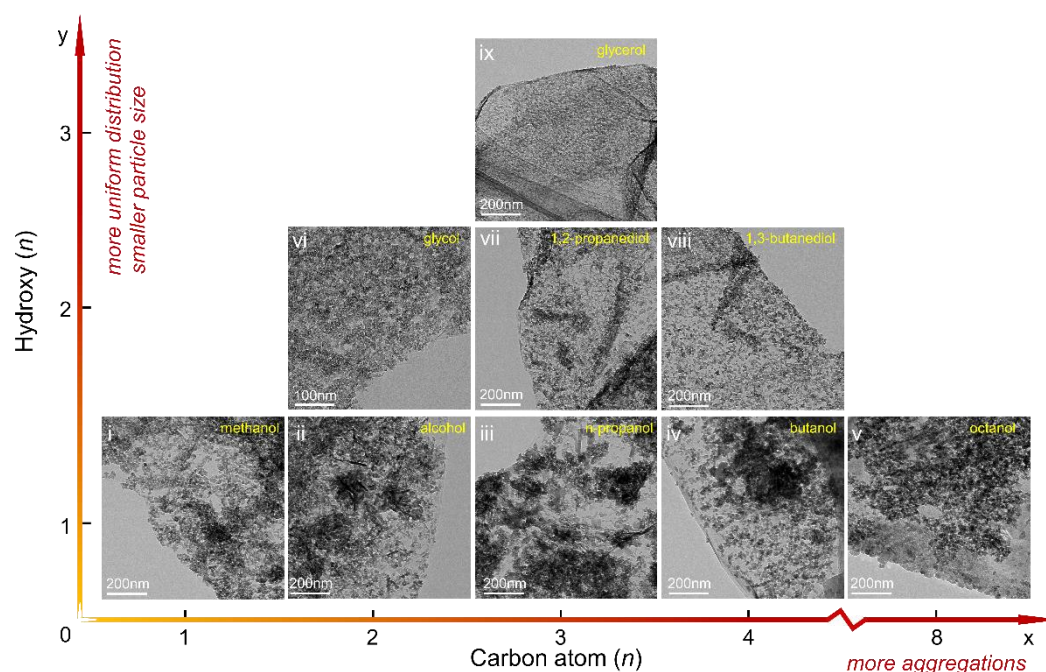
Figure S1. Low-resolution TEM images of Co-V-O nanodots on GO prepared at 180℃ in different alcohols solvents: methanol (i), alcohol (ii), n-propanol (iii), butanol (iv), octanol (v), glycol (vi), 1,2-propanediol (vii), 1,3-butanediol (viii), glycerol (ix).
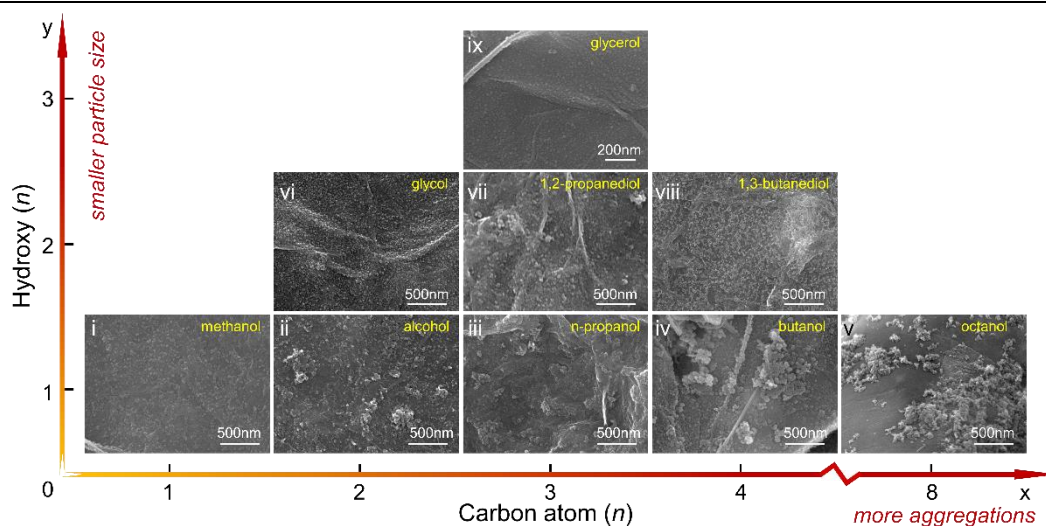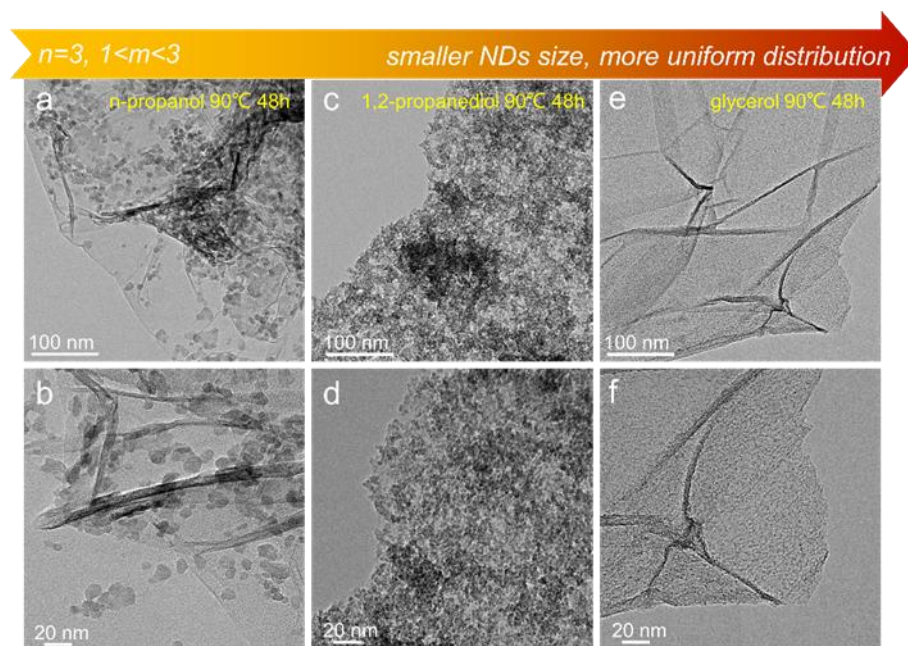
Figure S2. SEM images of Co-V-O nanodots on GO prepared at 180℃ in different alcohols solvents: methanol (i), alcohol (ii), n-propanol (iii), butanol (iv), octanol (v), glycol (vi), 1,2-propanediol (vii), 1,3-butanediol (viii), glycerol (ix).

Figure S3. TEM images of Co-V-O nanodots on GO prepared at 90℃ for 48h in n-propanol (a, b), 1,2-propanediol (c, d) and glycerol (e, f).
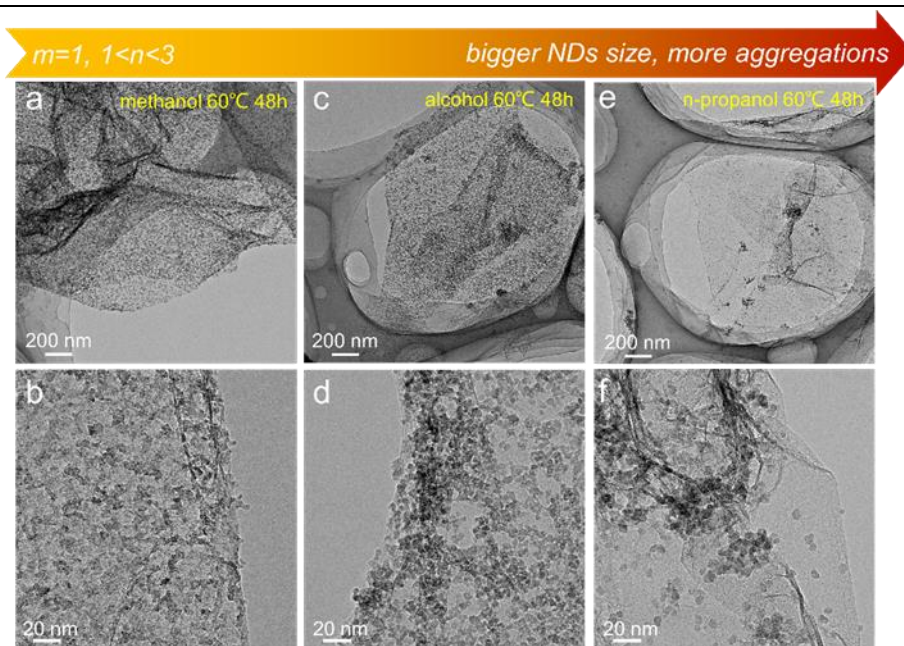
Figure S4. TEM images of Co-V-O nanodots on GO prepared at 60℃ for 48h in methanol (a, b), alcohol (c, d) and n-propanol (e, f).
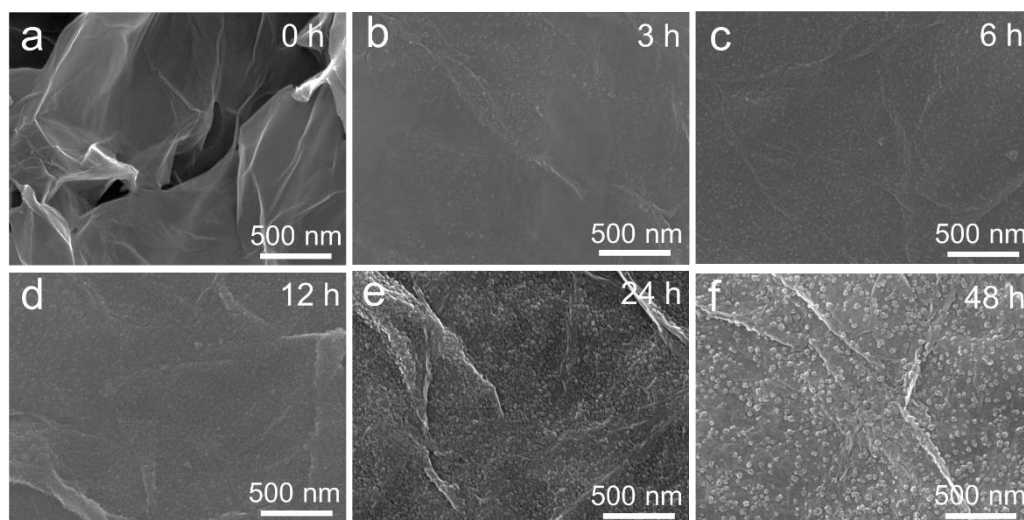

Figure S5. SEM images of Co-V-O nanodots on GO prepared at 180℃ in glycol at different times: 0 h (a), 3 h (b), 6 h (c), 12 h (d), 24 h (e), 48 h (f).
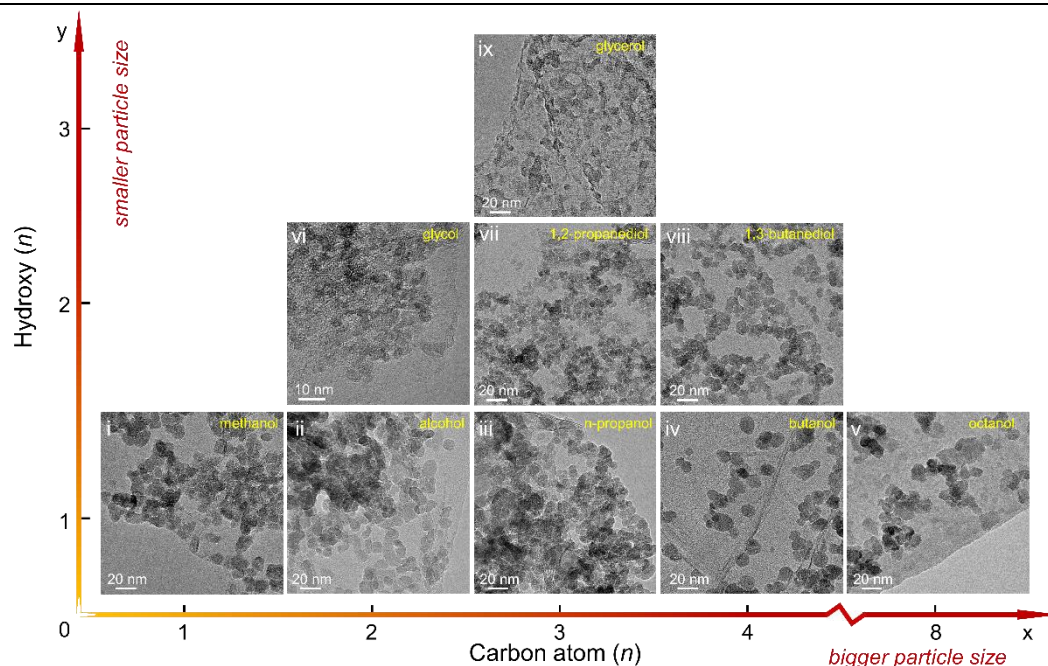
Figure S6. High-resolution TEM images of Co-V-O nanodots on GO prepared at 180℃ in different alcohols solvents: methanol (i), alcohol (ii), n-propanol (iii), butanol (iv), octanol (v), glycol (vi), 1,2-propanediol (vii), 1,3-butanediol (viii), glycerol (ix).
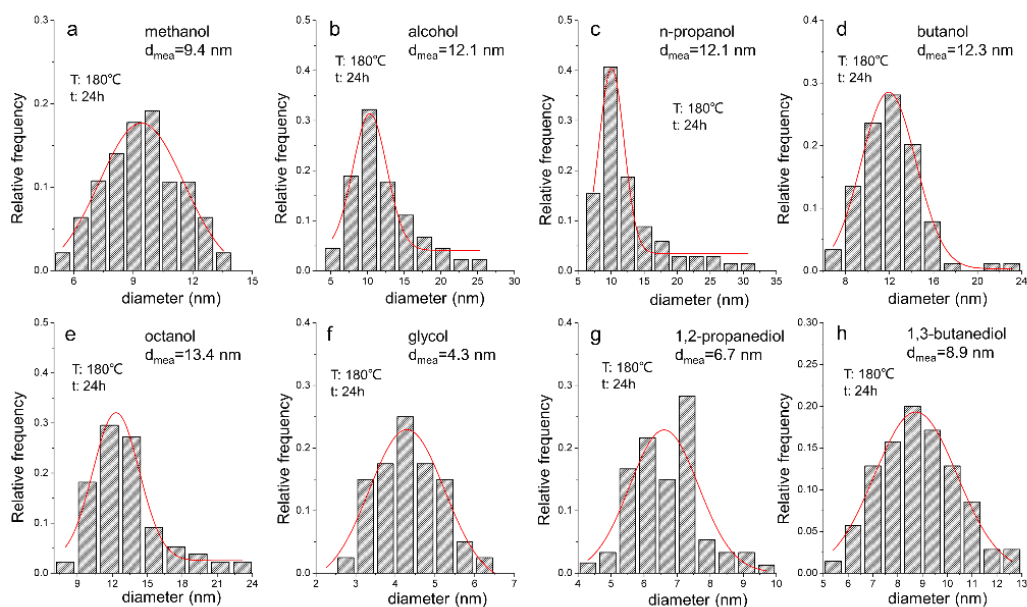

Figure S7. The diameters distributions of Co-V-O NDs on GO prepared at 180℃ in different alcohols solvents: (a) methanol, (b) alcohol, (c) n-propanol, (d) butanol, (e) octanol, (f) glycol, (g) 1,2-propanediol, (h) 1,3-butanediol.
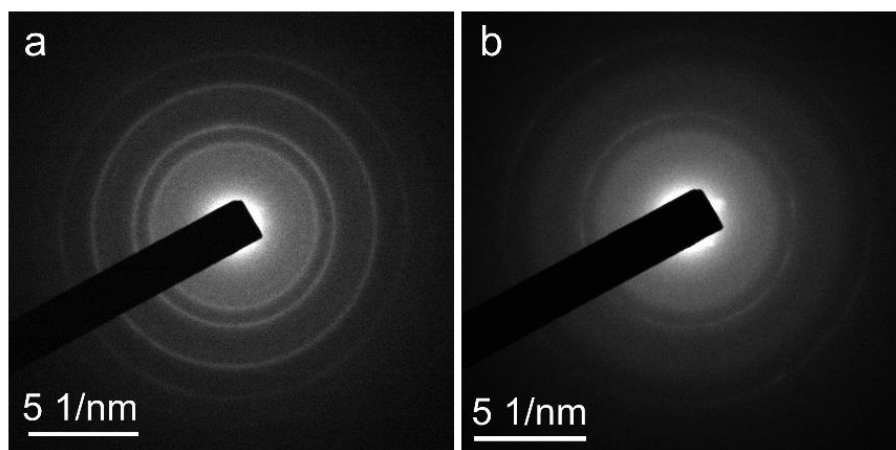
Figure S8. The SAED patterns of Co-V-O nanodots on GO prepared at 180℃ in glycol and glycerol solvents.
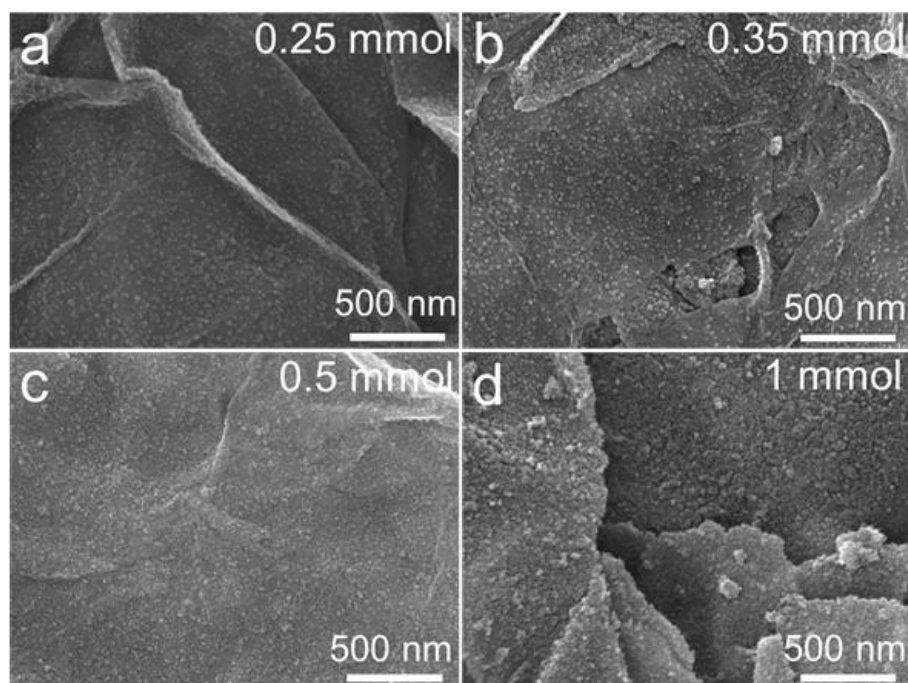

Figure S9. SEM images of Co-V-O NDs@GO prepared with different molar numbers at 180℃ in glycol: 0.25 mmol (a); 0.35 mmol (b); 0.5 mmol (c); 1.0 mmol (d).
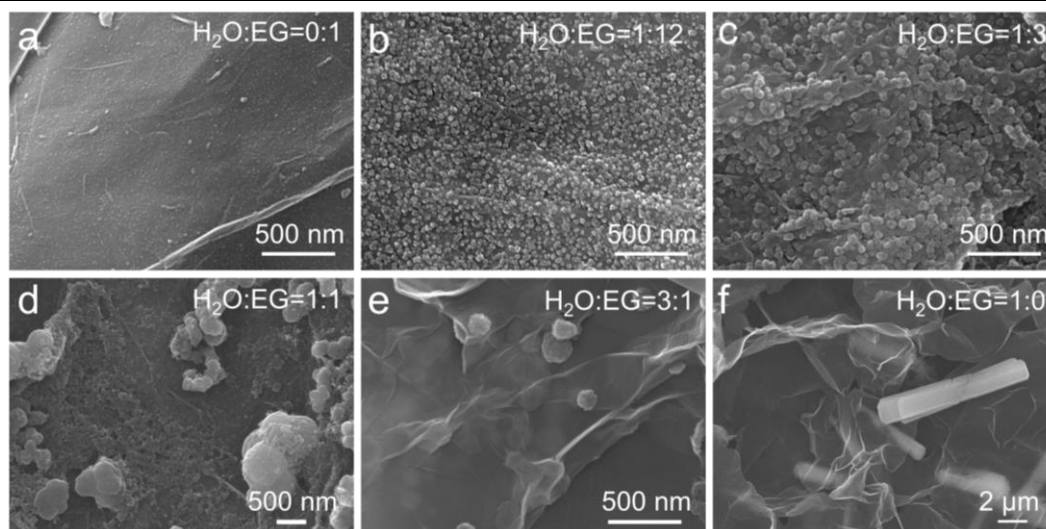
Figure S10. SEM images of Co-V-O nanodots on GO prepared at 180℃ in glycol/water solvents with different volume ratio (water: glycol): 0:1 (a), 1:12 (b), 1:3 (c), 3:1 (d), 3:1 (e), 1:0 (f). The freezing drying and re-dispersion of GO nanosheets in pure glycol were used to avoid the effect from water, while the Co-V-O NDs are much more fine and lower loading, compared with those samples prepared in the mixed solvents. With the increase of water contents, the diameters of Co-V-O gradually increase from several nanometers to a few hundred nanometers. This result indicates that the growth rates k could be controlled by adjusting the ratio of glycol/H_2O.
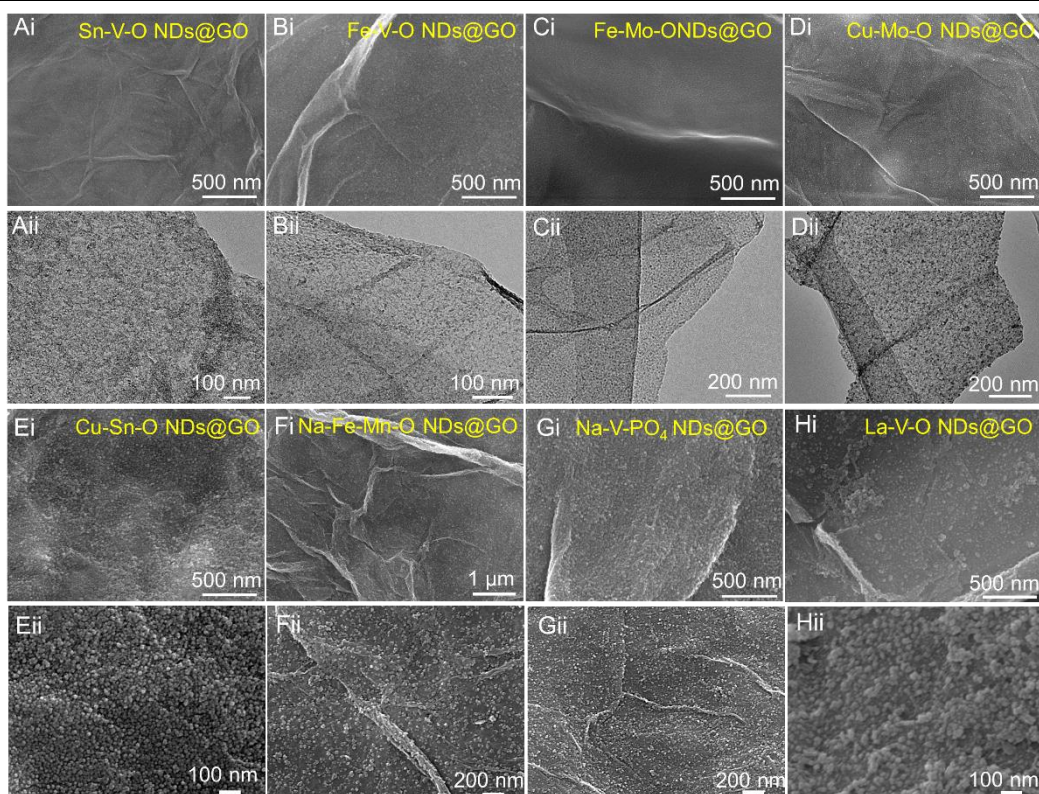
Figure S11. Morphologies of tin vanadate (Sn-V-O) nanodots (Ai, Aii), ferric vanadate (Fe-V-O) nanodots (Bi, Bii), iron molybdate (Fe-Mo-O) nanodots (Ci, Cii), copper molybdate (Cu-Mo-O) nanodots (Di, Dii), tin-copper oxide (Sn-Cu-O) nanodots (Ei, Eii), polymetallic oxide (Na-Fe-Mn-O) nanodots (Fi, Fii), phosphate (Na-V-PO$_4$) nanodots (Gi, Gii) and lanthanum vanadate (La-V-O) nanodots (Hi, Hii) on GO.
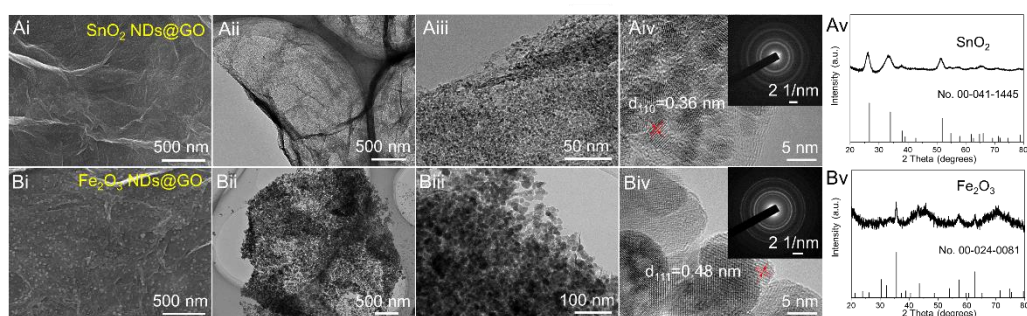

Figure S12. SEM, TEM, HRTEM (insets: SAED patterns) images and XRD patterns of SnO$_2$ NDs@GO (Ai-Av), Fe$_2$O$_3$ NDs@GO (Bi-Bv).
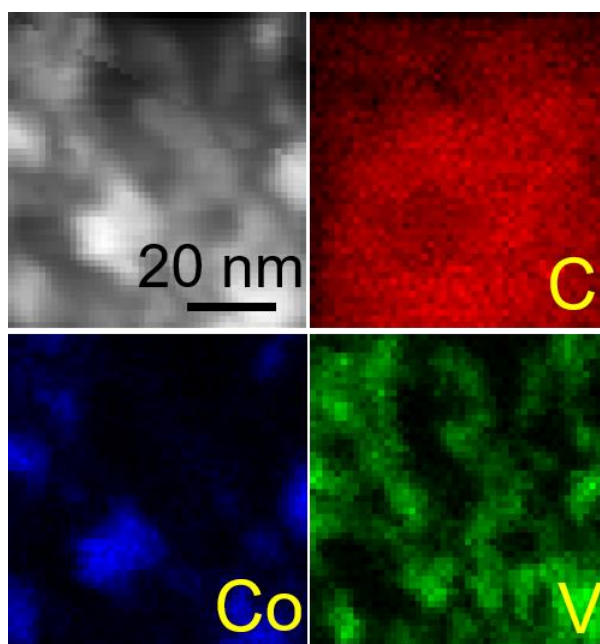
Figure S13. Elemental maps of C, Co and V in the Co/VN NDs@GO. The energy dispersive X-ray (EDX) elemental mappings of Co/VN NDs@GO show a strong V signal around metallic Co, which reveal the heterogeneous structure.
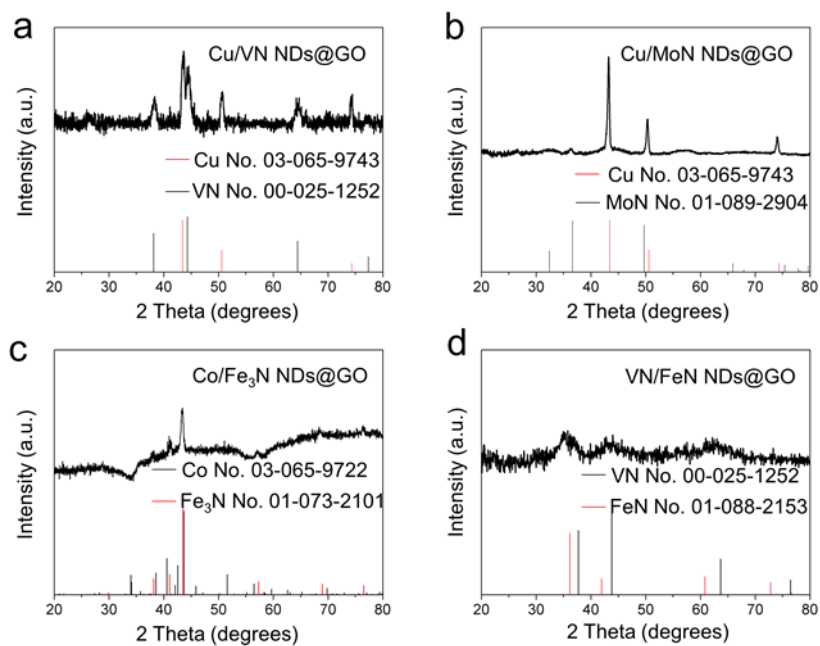

Figure S14. XRD patterns of Cu/VN NDs@GO (a), Cu/MoN NDs@GO (b), Co/Fe₃N NDs@GO (c), VN/FeN NDs@GO (d).
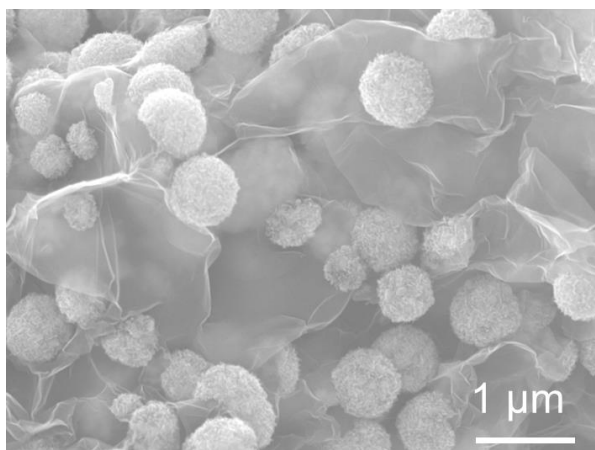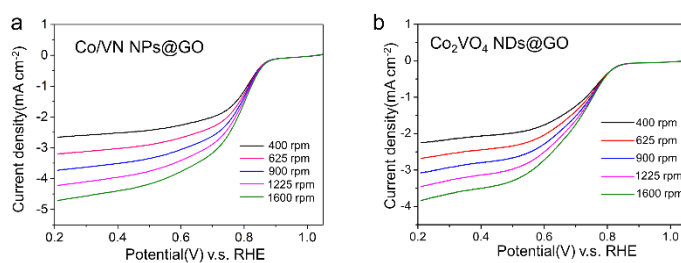
Figure S15. SEM image of Co/VN NPs@GO.

Figure S16. LSVs of (a) Co/VN NPs@GO; (b) Co$_2$VO$_4$ NDs@GO.
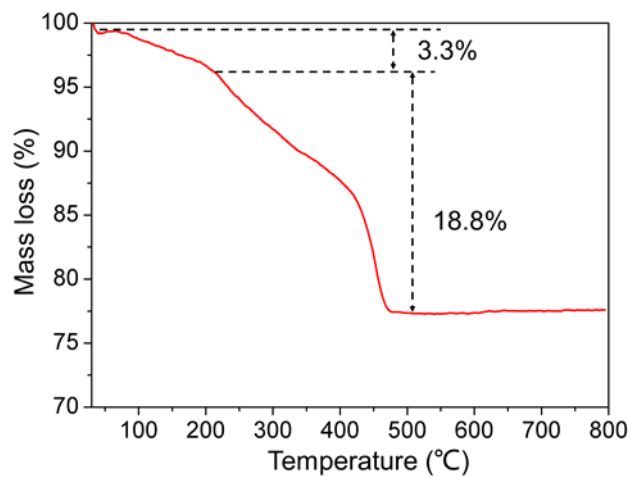

Figure S17. TG curve of Co$_2$VO$_4$ NDs@GO. The first step up to 211°C is attributed to the removal of 3.3 wt% absorbed water. The second step up to 480°C is caused by the oxidization of GO, indicating that the GO content is 18.8 wt%.
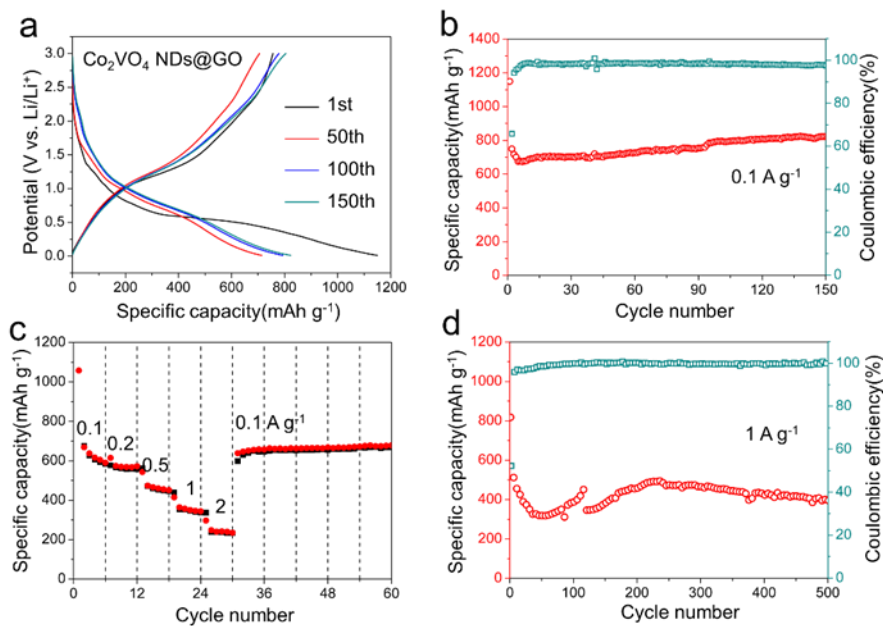
Figure S18. Electrochemical performance of Co₂VO₄ NDs@GO for LIBs: (a) Charge-discharge voltage profiles of at 0.1 A g^{-1}; (b) Cycling performance at 0.1 A g^{-1}; (c) Rate capability and (d) Cycling performance at 1 A g^{-1}.